

Long-time relaxation of ion-bombarded silicon studied with the kinetic activation-relaxation technique: Microscopic description of slow aging in a disordered system

Laurent Karim Béland* and Normand Mousseau†

Regroupement Québécois sur les Matériaux de Pointe (RQMP), Département de physique, Université de Montréal, Case Postale 6128, Succursale Centre-ville, Montréal, Québec H3C 3J7, Canada

(Received 11 September 2013; published 18 December 2013)

Diffusion and relaxation of defects in bulk systems is a complex process that can only be accessed directly through simulations. We characterize the mechanisms of low-temperature aging in self-implanted crystalline silicon, a model system used extensively to characterize both amorphization and return to equilibrium processes, over 11 orders of magnitudes in time, from 10 ps to 1 s, using a combination of molecular dynamics and kinetic activation-relaxation technique simulations. These simulations allow us to reassess the atomistic mechanisms responsible for structural relaxations and for the overall logarithmic relaxation, a process observed in a large number of disordered systems and observed here over the whole simulation range. This allows us to identify three microscopic regimes, annihilation, aggregation, and reconstruction, in the evolution of defects and to propose atomistic justification for an analytical model of logarithmic relaxation. Furthermore, we show that growing activation barriers and configurational space exploration are kinetically limiting the system to a logarithmic relaxation. Overall, our long-time simulations do not support the amorphous cluster model but point rather to a relaxation driven by elastic interactions between defect complexes of all sizes.

DOI: [10.1103/PhysRevB.88.214201](https://doi.org/10.1103/PhysRevB.88.214201)

PACS number(s): 61.72.uf, 61.43.Bn, 61.72.Cc, 79.20.Rf

I. INTRODUCTION

Understanding the aging of ion-implanted materials is a problem with important technological^{1,2} and fundamental implications.^{3,4} It bridges the gap between the physics of individual point defects and that of fully amorphous solids, in order to establish guiding principles in the analysis of disordered materials. Ion implantation of crystalline silicon (*c*-Si) at keV energies, which creates subamorphization damage, is a model problem that plays a role in microelectronic device fabrication⁵ and that can provide important insights about amorphization.^{6,7}

Not surprisingly, this system has been the object of a large number of numerical studies over the years, significantly increasing our microscopic understanding of the accumulation, thermodynamics, and kinetics of damaged and amorphous structures in ion-implanted Si. For instance, Caturla *et al.*⁸ studied, with molecular dynamics (MD), 5 keV and 15 keV implantations of As and Pt in *c*-Si, with simulations reaching 0.5 ns. They observe amorphous pockets that recrystallize, with barriers that grow with the amorphous pocket size. Jaraiz *et al.*,⁹ using a code based on Monte Carlo diffusion coupled to a binary collision approximation simulator, studied 40 keV self-implantation and annealing of Si at 1088 K, and found excess self-interstitial densities in good agreement with experimental data in the 10 s range. Hensel and Urbassek¹⁰ found that 10–100 eV implantation of Ar in Si is sufficient to induce long-lasting (over a day at room temperature) defects, although they do not show 5- and 7-rings typical of amorphous regions. Norlund *et al.*¹¹ performed 2 ns MD simulations, initialized at 0 K and rapidly quenched, of 0.5 to 10 keV Si self-implantations. They showed that about 50% of point defects (at 5 keV) aggregate in clusters of less than 6 defects (including isolated point defects). Extended amorphouslike pockets (more than 20 defects) are not present in the majority of the final states of their runs.

Near the turn of the century, Tang *et al.*¹² performed tight-binding MD simulations of the annihilation of isolated self-interstitials and vacancies in *c*-Si and observed a metastable configuration, analogous to the Wooten-Winer-Weaire bond defect.¹³ Further MD characterizations of these IV pairs by Marques *et al.*¹⁴ demonstrated that accumulation of these pairs led to increasingly stable clusters identified with an amorphous topology. Marques *et al.* also performed lattice-based kMC simulations centering on IV-pair diffusion and recombination described by a binary approximation simulator, predicting the presence and stability of amorphous zones in implanted *c*-Si in good agreement with experiments. More recently, Foiles¹⁵ performed a detailed analysis of the damage created by 10 ps NVE MD simulations initialized at room temperature of 25 eV to 25 keV Si self-implantations, observing that about two-thirds of the point defects created by the damage cascade are not surrounded by an amorphous local topology at 5 keV. Pothier *et al.*¹⁶ ran 1 ns MD simulations of 3 keV Si self-implantation and annealing at room temperature. They found that the potential energy drops in steps, associated with the coordinated recrystallization of several tens of atoms, and found that implantation of *a*-Si shares several similar feature with that of *c*-Si. Finally, Borodin¹⁷ performed 5 ns MD simulations of keV Si self-implantation at 1000 K, observing that damaged defective clusters rapidly transform into simpler complexes and point defects.

Overall these simulations have provided a great insight regarding the short-time annealing of ion-implanted *c*-Si, suggesting, in particular, that amorphous pockets are responsible for long-time relaxation and pointing to the importance of the interstitial-vacancy (IV) pair defect. To assess the validity of these suggestions, it is necessary to access a much longer time scale that is just now becoming available to off-lattice simulation. Indeed, in the past year,¹⁸ state-of-the-art atomistic simulations have permitted the observation, with atomistic details, of damage evolution on a time scale which permits

comparisons to experiments (on the order of a second, at room temperature). Indeed, we showed, using the kinetic activation-relaxation technique (k-ART),^{19,20} an off-lattice, self-learning kinetic Monte Carlo (kMC) algorithm, that it is possible to fully simulate the annealing of 3 keV Si self-implantation on time scales surpassing 1 s,²¹ with results in excellent agreement with nanocalorimetry experiments.¹⁸ The observed relaxation is logarithmic, with limiting activated events whose barriers grow as time evolves. We also showed that the kinetics can be explained by a two-step “replenish and relax” model where rate-limiting activated events unlock the system, replenishing the local energy landscape with heat-releasing events (with a uniform distribution of activation energy barriers), which is necessary for relaxation.

In this article, we characterize the atomistic details of this system. First, we investigate the regimes that appear during the time evolution of structural defects. Second, we present the atomistic relaxation mechanisms that were simulated by k-ART. Third, we characterize the nature of the limitations to relaxation rates. Fourth, we present an analytical account of our results. Finally, we discuss the physical significance of these results.

II. METHODOLOGY

Ion-implanted silicon is characterized by the presence of highly defective regions associated with atoms in off-lattice positions and related through long-range elastic stress fields. Its time evolution has been studied extensively using molecular dynamics.^{8–10,15–17} Due to computing costs associated with this technique, simulated time scales have been limited to 10 to 100 ns, sampling only the very onset of relaxation at room temperature,¹⁶ or involving annealing at high temperatures.¹⁷ Longer simulations were reached using standard lattice-based kMC methods.^{9,14} However, these impose two major approximations to allow the construction of a preliminary catalog: a lattice-based description that restricts seriously atomic positions and, at best, a continuum description of elastic deformations.^{4,7} These uncontrolled restrictions leave some questions as to the accuracy of these approaches, particularly regarding the local relaxation.¹⁸ The kinetic activation-relaxation technique (k-ART) lifts these limitations by removing the lattice requirements, fully incorporation short- and long-range elastic effects and building the event catalog on-the-fly.

k-ART uses the topology of the local environment surrounding each atom to classify configurations, with the help of the extensive NAUTY package,²² allowing the construction of an event catalog without any crystalline requirement. For generating new events and reconstructing old ones, it implements the activation-relaxation technique (ART *nouveau* or ARTn^{23,24}). ARTn is a very efficient open-ended searching algorithm for transition states that allows the identification of new events as the system evolves. At each step, therefore, events are reconstructed from the catalog, which is expanded when new topologies are found, and all barriers corresponding to 99.99% of the computed rate are fully relaxed, taking all elastic effects exactly into account both at minima and transitions states. k-ART was used with success to predict the structural evolution of vacancies in iron,²⁵ which was

independently verified by Xu *et al.*,²⁶ the structural relaxation of amorphous silicon,^{21,27} the kinetics of point defects in *c*-Si¹⁹ and *a*-Si,²⁸ and the measured heat release of ion-implanted *c*-Si in nanocalorimetry experiments.¹⁸ More details about the algorithm can be found in Refs. 19 and 27.

Three independently ion-implanted Stillinger-Weber silicon²⁹ models are prepared by implanting a 3 keV Si atom in a 120 000-atom slab and relaxing at 300 K for 1 to 10 ns using molecular dynamics (MD), following the procedure described in Ref. 16. A 27 000-atom cubic box containing the cascade-damage for each model is then removed from the slab and simulated, with periodic-boundary conditions, using k-ART. In total, 11 k-ART simulations are run from these three models for times ranging from 1 μ s to more than 1 s.

The final time scale is determined by the nature of the low-energy barrier states in each model. Indeed, kMC simulations are limited by the presence of low-energy nondiffusive barriers that consume the computer time without leading to structural evolution. In order to handle these so-called flickering states, or flickers, k-ART uses the autoconstructing basin mean-rate method (bac-MRM),¹⁹ based on the mean-rate method proposed by Puchala *et al.*³⁰ Successive flickering states are collected into a single basin, separated by a defined maximum energy barrier or energy threshold. As the bac-MRM finds new flickers, it creates a basin or adds it to an existing one. This basin is formally treated as a single minimum with the exit probability transitions computed analytically. Such an approach allows for a very efficient handling of flickers into k-ART.

Other mechanisms also slow down the dynamics. This is the case of the one-dimension fast “2I+IV” defect complex diffusion, associated with a 0.32 eV barrier and first observed by Marqués *et al.*³¹ The shortest k-ART simulations are all characterized by the presence of a high number of these fast diffusers that go round the box along the (111) axis without ever encountering a defect on which to anneal. Since these weakly interacting diffusers do not play a particular role in structural relaxation (other than diffusing matter), we focus the results section on the 6 simulations that reach and exceeded the 10 μ s time scale.

In order to analyze these processes, we identify point defects using a criterium loosely based on Lindemann spheres.^{10,32} All atoms near their perfect lattice positions, i.e., if the distance between their position and the lattice position is smaller than 0.5 Å, are considered as on-lattice. Atoms displaced by a larger distance are considered as self-interstitials. Unmatched atoms on the perfect lattice are considered to be vacancies. The positions of these point defects for typical configurations are illustrated in Fig. 1.

We analyze point defect clusters and complexes with the Hoshen-Kopelman algorithm.³³ We include single point defects and point defect complexes when computing the number of clusters and average cluster size.

III. RESULTS

Figure 2 shows the evolution of the relative energy as a function of time for the 11 k-ART simulations started from three different ion-implantation processes. They indicate that, for a given cascade, relaxation is close to logarithmic even

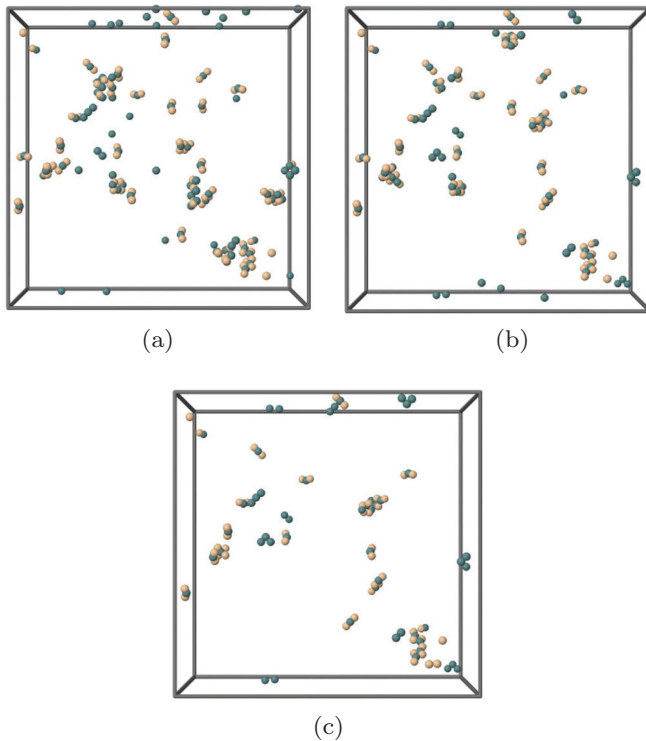


FIG. 1. (Color online) Illustration of point defects for typical configurations in a 27 000-atom system after different annealing times, for the same simulation, along with the number of point defects. (a) time = 10 ns, 184 point defects; (b) time = 74 μ s, 144 point defects; (c) time = 0.05 s, 104 point defects. Interstitials are colored in beige and vacancies in blue.

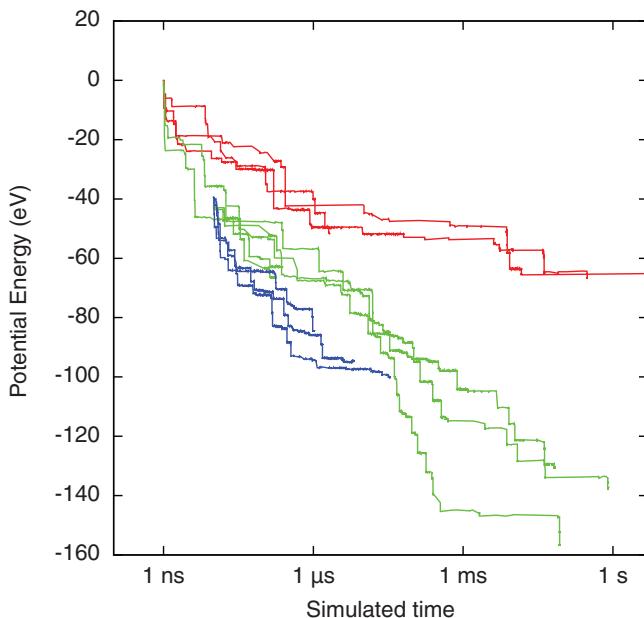


FIG. 2. (Color online) Time evolution of potential energy for k-ART simulations. The lines correspond to independent simulations starting from three different implantation runs.

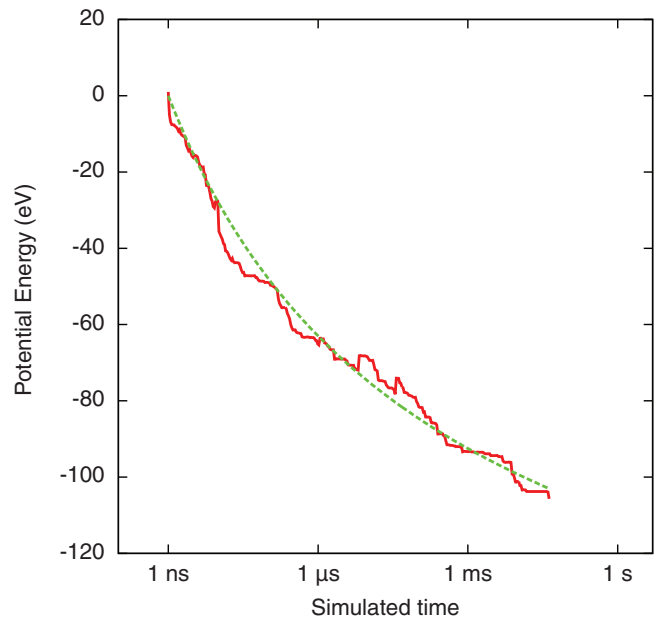


FIG. 3. (Color online) Red solid line: The potential energy of our simulations, averaged over the lines plotted in Fig. 2. Green dashed line: Solution of 1 at $T = 300$ K, with $h(E_b)n(E_b, t = 0) = 53E_b^{-1.7}$.

though a small curvature can be observed when the data are averaged (Fig. 3). With detailed information about the microscopic events leading to this long-time behavior, it is possible to understand the origin of the relatively common logarithmic relaxation.^{34–37} Logarithmic relaxation in this system is also observed in MD simulations,¹⁶ which serve as an input to our computations. In total, logarithmic relaxation lasts for at least 11 orders of magnitude of time.

Visual inspection of the system at 1 ns, as illustrated in Fig. 1, indicates that most large defect clusters (i.e., the so-called “amorphous pockets”¹⁴) are already annihilated, as described in Ref. 16. Most of the defects are either punctual or aggregated in small complexes. Indeed, the average defect cluster size, including point defects, is of 5 defects, which is not coherent with an amorphous pockets description. Visual inspection at 74 μ s in Fig. 1 leaves no room for ambiguity to the fact that no amorphous clusters are left. Nevertheless, logarithmic relaxation continues.

A. Evolution of structural defects

We present two descriptions of the collective and atomistic behavior of point defects. We first look at the collective regimes that lead to relaxation in individual simulations. We then look at the collective regimes that control the aggregate structural relaxation in many simulations (which is comparable to simultaneous ion implantations in nonoverlapping volumes, as in low-fluence ion bombardment). This time evolution can be classified into three regimes. If the average defect cluster (or complex) size increase, with no change in the number of defects, the system is aggregating defects. If the number of defects and the average cluster size both increase, the system is experiencing reconfiguration. If the number of point defects decreases, the system is annihilating (or recombining) point defects.

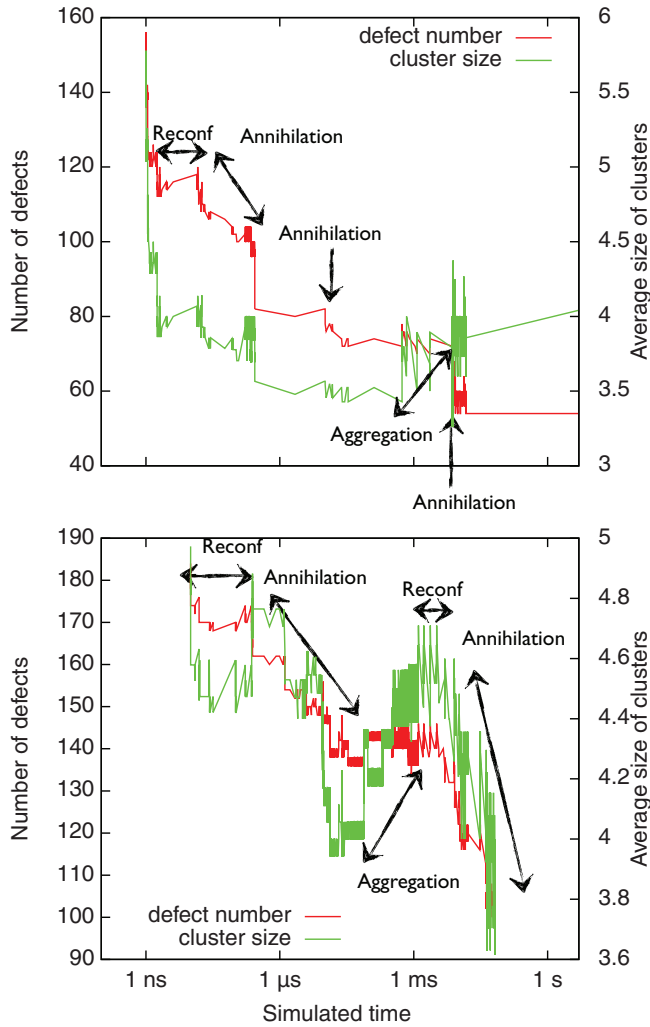


FIG. 4. (Color online) The time evolution of the total number of point defects (in red, left scale) and the average defect cluster size (in green, right scale) in two independent simulations. As indicated in the panels, the time evolution goes through a number of recombination, aggregation, and reconfiguration regimes.

We illustrate the collective behavior of point defects in individual k-ART runs in Fig. 4. It shows the time evolution of both the total number of point defects and the average cluster size in a 1 s (top panel) simulation and a 0.066 s simulation (lower panel).

The top panel is associated with the run plotted as the red line that crosses 1 s in Fig. 2. The potential energy relaxation, as seen in Fig. 2, takes place by steps, with some very steep cliffs separated by long periods of time with little structural relaxation. The evolution of the number of point defects and the size of clusters exhibits a similar behavior. We see a large decrease in the number of defects, cluster size, and potential energy between 1 and 2 ns, followed by a small increase in both the number of defects and cluster size between 2 and 15 ns, which corresponds to a reconfiguration regime, which does not contribute to potential energy relaxation. Between 15 and 275 ns, and between 10 and 36 μ s, relaxation is dominated by defect annihilation that is accompanied by a significant decrease in the potential energy. From 0.5 ms to 7.5 ms, the

average cluster size increase with a constant number of defects and a 4.5 eV decrease in potential energy, which corresponds to an aggregation regime. We observe two final recombination events at 7.5 ms and 8.5 ms.

In the bottom panel of Fig. 4, we plot the same quantities as in the top panel for the k-ART run illustrated as the green line in Fig. 2 characterized by a final potential energy value of -131 eV at 66 ms. The decrease in potential energy is spread out much more evenly across time intervals than in the run illustrated in the top panel of Fig. 4. Also, we observe more contrasted and long-lasting regimes of reconfiguration, aggregation, and recombination (annihilation) of point defects. At short times, below about 100 ns, reconfiguration events dominate as the average cluster size and number of point defects are stable. The potential energy declines by less than 1 eV. After 100 ns, defects annihilate steadily before reaching a plateau, at 100 μ s, leading to a drop in cluster size. As these small clusters are mobile, complex rearrangements between 100 μ s and 4 ms lead to a sharp increase in the average cluster size from 4 to 4.7, while the number of defects remains, corresponding to an aggregation phase. In the last phase, lasting to the end of the simulation at 100 ms, both the number of defects and cluster size decrease, signature of a collective annihilation regime.

We can also characterize the aggregate behavior of point defects by plotting the average cluster size and the average total number of defects for all k-ART runs, as shown in Fig. 5, with the average potential serving as an indication of the overall relaxation level. In the top panel, we see that the number of defects decreases monotonically (a few discontinuities are associated with the fact that not all simulations are the same length in time). The potential energy and the number of defects follow a similar trend indicating that defect annihilation dominates the energy release. In the lower panel, the average size of point defect clusters decreases mostly

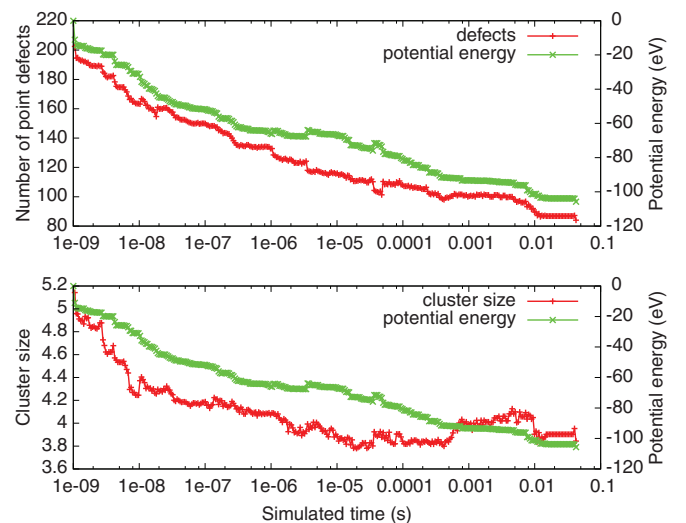


FIG. 5. (Color online) Top: The number of point defects, averaged over all simulations. Bottom: The size of defect clusters and complexes, averaged over all simulations. In both panels, the averaged potential energy is plotted as an indicator of the degree of structural relaxation.

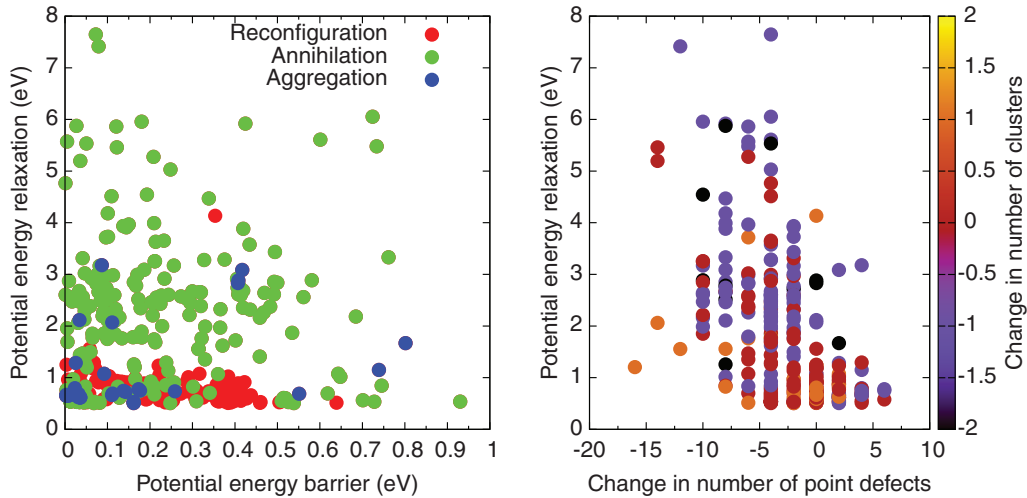


FIG. 6. (Color online) Left: Potential energy relaxation as a function of activation barrier height for each event releasing more than 0.5 eV, aggregated over all k-ART runs. The color indicates the type of relaxation event. Right: Potential energy relaxation as a function of the change in the number of point defects for each event releasing more than 0.5 eV, aggregated over all k-ART runs. The coloring indicates the change in the number of clusters caused by the relaxation event.

monotonically until about 100 μ s. After a relatively long plateau, the average cluster size increase rapidly around 1 ms. This increase is not an artifact of some simulations ending abruptly. The correlation between the decrease in cluster size and the potential energy is not as remarkable as the correlation between the number of point defects and potential energy. This indicates that aggregation does not play a role as important as annihilation in heat release, a point further discussed below. Overall, the aggregate behavior of cluster size is quite different from the behavior of individual cascades. Indeed, Fig. 4 shows that the cluster size of an individual cascade can exhibit large variations, which is not the case in aggregate. Finally, the bump in cluster size from 0.3 ms to 100 ms is associated with a plateau in the number of point defects and a cluster reorganization leading to a slow energy relaxation. Thus, some of the overall behavior is linked with specific time scale and not simply the details of the initial configuration.

B. Relaxation events

In this section, we examine the contribution of individual events to energy relaxation and the atomistic changes brought by each individual event. These correspond to the abrupt changes in potential energy shown in the top panel of Fig. 2. We aggregated events that were separated by less than 1 ps. Of these aggregated events, only those with an energy release of 0.5 eV or more were considered to avoid taking into account oscillations (flickers) with an amplitude smaller than 0.5 eV, which are common for $t > 10 \mu$ s.

For simplicity, these atomistic events are classified as in the previous section: recombination (or annihilation) events, aggregation events, and reconstruction events. For example, recombination events occur both in small clusters and in point defect complexes such as the well-known, but not experimentally observed, I-V pair.^{12,38} It is important to note that while we classify energy relaxation events using the same three names as the regimes of structural time evolution

of defects, structural relaxation events of all classes happen during any structural evolution regime. For instance, the aggregation regime in the bottom panel of Fig. 4 is in fact a succession of atomistic annihilation and reconfiguration events that result in an increasing average cluster size and a constant number of defects.

Figure 6 shows the energy released by each individual event in all the simulations. They are plotted in the left panel as a function of the activation barrier height and colored as a function of their classification. They are plotted in the right panel as a function of the change in the number of point defects, colored as a function of the change in the number of clusters. We observed 350 exothermic events in total. There is no clear relationship between the activation barrier height and the potential energy relaxation of each event, in agreement with Ref. 39.

142 (41%) events conserve or increase the number of point defects (i.e., reconfiguration or aggregation events), releasing no more than 4.2 eV (120 of these events release less than 1.2 eV). 83 of these keep the number of clusters constant (reconfiguration), 27 increase it (reconfiguration), and 32 decrease it (aggregation). 208 (59%) events decreased the number of point defects (i.e., recombination); 106 of these events decrease the number of clusters, 85 keep the number of clusters constant, while 17 increase the number of clusters. 97 of the recombination events involve the annihilation of 4 point defects, such as the IV pair. In the absence of other nearby defects, we report an energy barrier to bond defect recombination in agreement with the literature (0.43 eV). Accumulation of these bond defects does not necessarily lead to the higher recombination barrier postulated by nucleation theory; it depends rather on the precise orientation of the defect cluster at hand. The effect can increase, decrease, or have no impact on the stability of the bond defect, as is seen in the left panel of Fig. 6. Indeed, the annihilation events, shown in green, display a wide range of potential energy barriers.

On average, aggregation events have an activation barrier of 0.17 eV, reconfiguration events a barrier of 0.23 eV, and annihilation events a barrier of 0.22 eV. As for the average potential energy relaxation, it is of 1.12 eV for aggregation events, 0.81 eV for reconfiguration events, and 2.23 eV for annihilation events.

In total, aggregation accounts for 9% of exothermic events and 6% of potential energy relaxation, reconfigurations for 31% of exothermic events and 15% of potential energy relaxation, and recombination for 59% of events and 79% of potential energy relaxation.

C. Rate-limiting processes

The structural relaxation of implanted *c*-Si is logarithmic, which means that relaxation becomes increasingly kinetically limited as time progresses. There are two main classes of kinetic limitations. The first is the presence of rate-limiting activated processes with increasingly high barriers. As shown in the previous account of our computations,¹⁸ such events do take place in our simulations, and are necessary to unlock the system, replenishing the basin of heat-releasing events in the local energy landscape. The second class of kinetic limitation is related to the size of the locally explored energy basin where a large number of configurations are available, but only a very small fraction of those lead to relaxation. The system will thus spend a significant amount of time exploring these states, without any potential energy relaxation. The time spent exploring the landscape will reduce the rate of relaxation, as would an activated event with a high barrier.

As shown in Fig. 7, for any time interval, the energy barriers for the realized event are distributed quasicontinuously, with no specific value standing out in spite of the overall crystalline nature of the system. While activated events with the largest

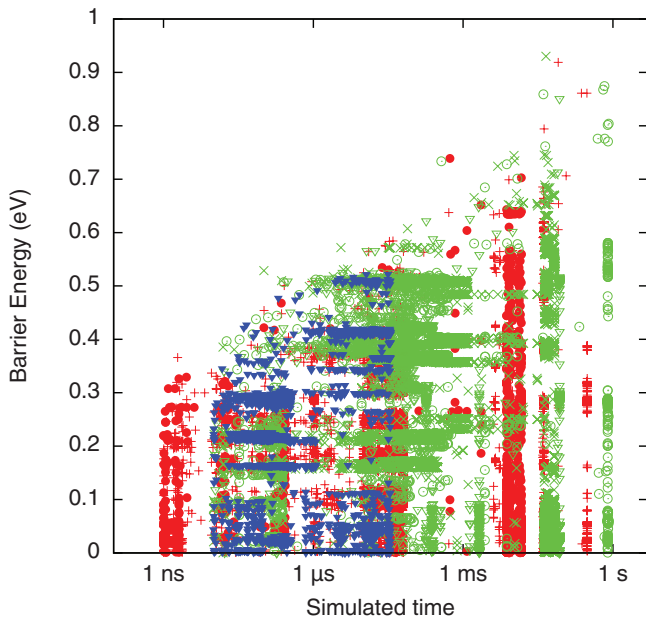


FIG. 7. (Color online) The potential energy barrier of activated events during k-ART runs. The color of the points indicate the corresponding runs in Fig. 2.

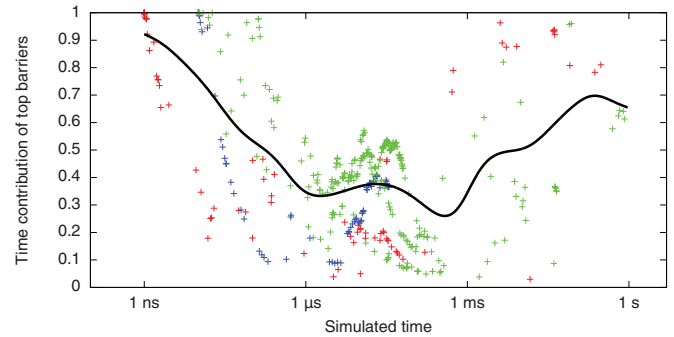


FIG. 8. (Color online) Proportion of total simulated time accounted for by the events with barriers that lie in the top 10% of the barriers executed in a small $\log(t)$ interval. The different points are from different simulations. The thick black line is an average.

energy barriers in each time frame are candidates as kinetically limiting event, the continuous spectrum suggests the existence of time regimes dominated by the exploration of specific energy basins.

In order to account for both classes of kinetic limitations, we compute the proportion of total simulated time accounted for by the events with barriers that lie in the top 10% of the barriers executed in a small interval on a logarithmic scale as the simulations progress in time. These proportions are illustrated in Fig. 8, for all simulations that reached 10 μ s. We also plot the average as a thick black line. The top 10% events account for 30% to 90% of the simulated clock as runs progress. The trend is U shaped, with maxima near 1 ns and 0.1 s. The minimum is reached between 1 μ s and 1 ms. Thus, the time spent to explore the landscape seems to be very significant between 1 μ s and 1 ms. These are the characteristic times for the diffusion of monovacancies, depending on the strain exerted on them by various defect complexes, which means a large configurational space is locally available to the system. In the other time domains, the system is mostly limited by rare activated events, which are necessary to unlock and replenish the energy landscape.

D. A continuum model for energy relaxation

Figure 2 shows the potential energy of all the k-ART runs as a function of time. The logarithmic decay is observable in each run. This type of decay is coherent with the long-tailed heat release measured by nanocalorimetry.^{7,18,40,41} We consider activated processes with an initial density of processes $n(E_b, t = 0)$ that are activated by first-order kinetics, that each release $h(E_b)$ heat, where E_b is the activated event's effective potential energy barrier. Events with a given E_b should be described by a Poisson process.⁴⁰ The heat released between E_b and $E_b + dE_b$ during the time interval between t and $t + dt$ is then written as

$$h(E_b)dn(E_b, t)dE_b = -h(E_b)n(E_b, t)ve^{-E_b/kT} dE_b dt. \quad (1)$$

By solving this equation at fixed or increasing temperatures, we can model constant temperature or temperature-dependent signals. If $h(E_b, t = 0)n(E_b)$ varies slowly, solving the equation at fixed temperature results in logarithmic decay of the potential energy, with $-h(E_b)n(E_b, t = 0)$ as the slope of the potential

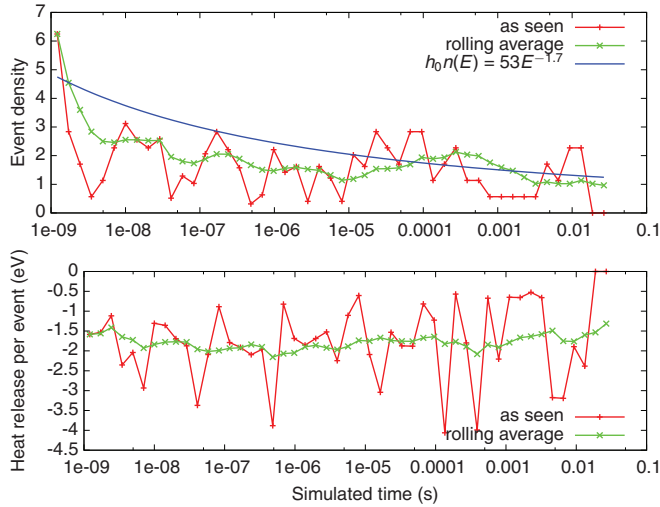


FIG. 9. (Color online) Top: The density, per log(time), of events that release more than 0.5 eV of heat. The red crosses are the data as is, the green x's are a rolling average over 10 points, and the blue curve is the density of events implied by $h_0 n(t = 0) = 53 E_b^{-1.7}$, with $h_0 = 1.7$ eV, as computed from the bottom panel. Bottom: The average heat released (potential energy relaxation) by events that release more than 0.5 eV of heat. The red crosses are the data as is; the green x's are a rolling average over 10 points.

energy with regards to $\log(\text{time})$.^{41,42} When solved with a constant increasing temperature, this slope determines the heat release measured by nanocalorimetry at temperature T_{E_b} corresponding to the characteristic E_b , following Arrhenius dependence. A proper description of $h(E_b)$ and $n(E_b, t = 0)$ is thus crucial to properly compare simulations and experiments.

To quantify the contribution of $h(E_b)$ and $n(E_b, t = 0)$, we identify individual heat-releasing events in each simulation. As explained in the previous section, we take into account all events that generate more than 0.5 eV of heat. The event density evolution is equivalent to $n(E_b, t = 0)$ and its heat release can then be computed.

Figure 9 illustrates the observed behavior averaged over our runs. The data were obtained by binning the results of all the simulations into regular $\log(t)$ intervals. The results, drawn with red crosses, are noisy but show a clear trend that is most evident with a rolling average over 10 points. The heat release (potential energy relaxation) oscillates around a constant value of 1.7 eV but remains time independent. We infer that relaxation events emit a random amount of heat, with a distribution centered around h_0 , a constant independent of E_b . This is in agreement with computations by Kallel *et al.* in *a*-Si, that do not observe correlation between the heights of the forward and reverse activation barriers.³⁹ The event density, however, decreases over time, more rapidly in first nanoseconds and slowing down afterwards: the rolling average (green line) is 6.2 events per $\log(t)$ at $t = 1.2$ ns falling to 2.5 events per $\log(t)$ at $t = 20$ ns and 0.96 events per $\log(t)$ at $t = 0.027$ s.

Equation (1) can thus be solved posing $h(E_b) = h_0 = 1.7$ eV and $n(E_b, t = 0) = n_0 E_b^\mu$, fitting the exponent μ and the constant n_0 so to describe the potential energy of our k-ART runs, averaged over all 11 simulations, as plotted in

Fig. 3. $\mu = -1.7$ and $h_0 n_0 = 53$ produce a good fit (see the blue curve in the top panel of Fig. 9). When solving at an increasing temperature, these values predict a heat signal in good agreement with nanocalorimetry experiments.¹⁸

IV. DISCUSSION

Investigation of the nature of heat-releasing events revealed that isolated events involving annihilation, aggregation, and reconfiguration all contribute to the total potential energy relaxation of the system, with recombination accounting for 59% of these events and 79% of potential energy relaxation. Once again, we stress that the succession of heat-releasing events can lead to a variety of structural evolution regimes with an overall effect on the distribution of defects that might differ from that of individual events.

A noticeable feature of these events is the nearly continuous distribution of the potential energy relaxation involved. This complex energy landscape is the result of the presence of point defects and small defect clusters and complexes. Indeed, multi-IV-pair clusters are absent from the simulation. Thus, relaxation cannot be described by the size of post-implantation amorphous clusters, as in the IV-pair model,¹⁴ but rather by taking into account elastic interactions between point defects and small defect complexes. Nevertheless, activated exothermic events exhibit a wide range of activation barriers and heat release per event, as is observed in severely disordered systems, such as *a*-Si⁴⁰ or polymer glasses.³⁵

Logarithmic decay is coherent with the potential energy relaxation observed by previous MD studies, that typically follow relaxation over three orders of magnitudes in time.^{8,10,15–17} This relaxation and the spread in the height of activation barriers was generally associated with the annealing of amorphous clusters. Here, we show that the logarithmic relaxation persists for at least nine orders of magnitudes in time even in the absence of amorphous clusters (i.e., after their annihilation).

In the case of individual implantations, the logarithmic decrease in potential energy is observed in tandem with three regimes of time evolution of defects: recombination (or annihilation), aggregation, and reconfiguration. The exact sequence of these regimes is somewhat stochastic, dependent on the kinetic path chosen by the ion-bombarded system. The annihilation regime is most often associated with potential energy relaxation, although aggregation regimes play a smaller role. As for regimes involving reconfigurations, they do not contribute much to potential energy relaxation, but play an important role in logarithmically limiting relaxation.

When considering many simultaneous implantations, we observe a steady decline of the number of defects (an annihilation regime) during most of the relaxation, with a short aggregation regime from 0.3 ms to 100 ms. To our knowledge, this is the first report explaining the full atomistic details on these time scales of time-evolution of point defect structures after ion-implantation and of the potential energy relaxation it produces, taking into account off-lattice configurations. While Refs. 9 and 14 report aggregation and annihilation of vacancies and interstitials, they do not report reconfiguration, nor the alternance of regimes. The variety of these regimes, and the fact that their concatenation leads to nearly logarithmic

relaxation, is an indication of the high level of disorder that the long-range interaction of defects can induce to the potential energy landscape.

Concerning rate-limiting processes, it is rather surprising that configurational space exploration and high-barrier events both have a significant role to play in logarithmically limiting the relaxation in the majority of time frames. It would be interesting to further investigate this issue in other logarithmically relaxing systems. Furthermore, the fact that barriers that unlock the system, and permit the replenish and relax¹⁸ behavior in *c*-Si, increase logarithmically raises questions: Were these barriers randomly distributed in such a manner at the beginning of the anneal, as proposed by the Gibbs model,⁴³ or is there a relationship between the order parameters and the unlocking barrier height (as proposed in Refs. 35,44–46)? Further work is needed to clarify this issue.

The fact that a largely crystalline system can exhibit an energy landscape similar to that in disordered systems warrants investigation. Why does keV implanted *c*-Si and *a*-Si exhibit similar heat release signatures during aging,^{7,16,47} but converge towards different order parameter values? A study involving reimplantation of our samples and their eventual amorphization could provide interesting insights about this issue.

V. CONCLUSION

Crystalline silicon implanted at low-keV energies is a model system for partially disordered systems, and defects dynamics, aging, and relaxation. We used the kinetic activation-relaxation technique to determine the kinetics of this system as it

logarithmically converges to its equilibrium state, i.e., the perfect lattice state. By closely tracking all activated events in second-long simulations, we identify individual relaxation mechanisms that account for the path towards equilibrium as well as relaxation regimes that emerge from the sequences of these individual events. This analysis also directly assesses the relative role of configurational space exploration and activation barriers, revealing that both are important to limit this system to a logarithmic relaxation rate. Furthermore, our simulations provide evidence to the claim that the degree of disorder does not affect the mean energy released by each relaxation event, but that it does change the density of relaxation events in a given time frame. This evidence is the basis for an analytical description of the relaxation of this disordered system. Finally, detailed analysis of the atomistic relaxation mechanisms demonstrates that “amorphous pockets” do not account for the complex mechanisms at hand. Rather, the logarithmic relaxation, a signature of disordered materials, is driven by elastic interactions between small defect complexes and point defects.

ACKNOWLEDGMENTS

We thank François Schiettekatte, Jean-François Joly, and Mickael Trochet for insightful discussions. This work has been supported by grants from the Natural Sciences and Engineering Research Council of Canada (NSERC) and the Fonds de Recherche du Québec Nature et les Technologies (FRQNT). We are grateful to Calcul Québec for generous allocations of computer resources.

*laurent.karim.beland@umontreal.ca

†normand.mousseau@umontreal.ca

¹A. Krasheninnikov and K. Nordlund, *J. Appl. Phys.* **107**, 071301 (2010).

²J. Srour and J. Palko, *IEEE Trans. Nucl. Sci.* **60**, 1740 (2013).

³G. Hobler and G. Otto, *Mater. Sci. Semicond. Process.* **6**, 1 (2003).

⁴L. Pelaz, L. Marqués, M. Aboy, P. López, and I. Santos, *Eur. Phys. J. B* **72**, 323 (2009).

⁵L. Rubin and J. Poate, *Ind. Phys.* **9**, 12 (2003).

⁶L. Pelaz, L. A. Marqués, and J. Barbolla, *J. Appl. Phys.* **96**, 5947 (2004).

⁷Y. Anahory, Ph.D. thesis, Université de Montréal, 2011.

⁸M.-J. Caturla, T. Díaz de La Rubia, L. Marqués, and G. Gilmer, *Phys. Rev. B* **54**, 16683 (1996).

⁹M. Jaraiz, G. Gilmer, J. Poate, and T. D. De La Rubia, *Appl. Phys. Lett.* **68**, 409 (1996).

¹⁰H. Hensel and H. M. Urbassek, *Phys. Rev. B* **57**, 4756 (1998).

¹¹K. Nordlund, M. Ghaly, R. Averback, M. Caturla, T. Diaz de La Rubia, and J. Tarus, *Phys. Rev. B* **57**, 7556 (1998).

¹²M. Tang, L. Colombo, J. Zhu, and T. Diaz de la Rubia, *Phys. Rev. B* **55**, 14279 (1997).

¹³F. Wooten, K. Winer, and D. Weaire, *Phys. Rev. Lett.* **54**, 1392 (1985).

¹⁴L. A. Marqués, L. Pelaz, M. Aboy, L. Enríquez, and J. Barbolla, *Phys. Rev. Lett.* **91**, 135504 (2003).

¹⁵S. M. Foiles, *Nucl. Instrum. Methods Phys. Res., Sect. B* **255**, 101 (2007).

¹⁶J.-C. Pothier, F. Schiettekatte, and L. J. Lewis, *Phys. Rev. B* **83**, 235206 (2011).

¹⁷V. Borodin, *Nucl. Instrum. Methods Phys. Res., Sect. B* **282**, 33 (2012).

¹⁸L. K. Béland, Y. Anahory, D. Smeets, M. Guihard, P. Brommer, J.-F. Joly, J.-C. Pothier, L. J. Lewis, N. Mousseau, and F. Schiettekatte, *Phys. Rev. Lett.* **111**, 105502 (2013).

¹⁹L. K. Béland, P. Brommer, F. El-Mellouhi, J.-F. Joly, and N. Mousseau, *Phys. Rev. E* **84**, 046704 (2011).

²⁰F. El-Mellouhi, N. Mousseau, and L. J. Lewis, *Phys. Rev. B* **78**, 153202 (2008).

²¹N. Mousseau, L. K. Béland, P. Brommer, J.-F. Joly, F. El-Mellouhi, E. Machado-Charry, M.-C. Marinica, and P. Pochet, *J. At., Mol., Opt. Phys.* **2012**, 925278 (2012).

²²B. D. McKay, *Congressus Numerantium* **30**, 45 (1981).

²³R. Malek and N. Mousseau, *Phys. Rev. E* **62**, 7723 (2000).

²⁴E. Machado-Charry, L. K. Béland, D. Caliste, L. Genovese, T. Deutsch, N. Mousseau, and P. Pochet, *J. Chem. Phys.* **135**, 034102 (2011).

²⁵P. Brommer and N. Mousseau, *Phys. Rev. Lett.* **108**, 219601 (2012).

²⁶H. Xu, R. E. Stoller, and Y. N. Osetsky, *J. Nucl. Mater.* **443**, 66 (2013).

- ²⁷J.-F. Joly, L. K. Béland, P. Brommer, F. El-Mellouhi, and N. Mousseau, *J. Phys.: Conf. Ser.* **341**, 012007 (2012).
- ²⁸J.-F. Joly, L. K. Béland, P. Brommer, and N. Mousseau, *Phys. Rev. B* **87**, 144204 (2013).
- ²⁹F. H. Stillinger and T. A. Weber, *Phys. Rev. B* **31**, 5262 (1985).
- ³⁰B. Puchala, M. L. Falk, and K. Garikipati, *J. Chem. Phys.* **132**, 134104 (2010).
- ³¹L. A. Marqués, L. Pelaz, J. Hernández, J. Barbolla, and G. H. Gilmer, *Phys. Rev. B* **64**, 045214 (2001).
- ³²F. A. Lindemann, *Phys. Z* **11**, 609 (1910).
- ³³J. Hoshen and R. Kopelman, *Phys. Rev. B* **14**, 3438 (1976).
- ³⁴G. B. McKenna, *J. Phys.: Condens. Matter* **15**, S737 (2003).
- ³⁵A. Knoll, D. Wiesmann, B. Gotsmann, and U. Duerig, *Phys. Rev. Lett.* **102**, 117801 (2009).
- ³⁶A. Sepúlveda, E. Leon-Gutierrez, M. Gonzalez-Silveira, C. Rodríguez-Tinoco, M. T. Clavaguera-Mora, and J. Rodríguez-Viejo, *Phys. Rev. Lett.* **107**, 025901 (2011).
- ³⁷A. Amir, Y. Oreg, and Y. Imry, *Proc. Natl. Acad. Sci. USA* **109**, 1850 (2012).
- ³⁸L. Pelaz, L. A. Marqués, M. Aboy, J. Barbolla, and G. H. Gilmer, *Appl. Phys. Lett.* **82**, 2038 (2003).
- ³⁹H. Kallel, N. Mousseau, and F. Schiettekatte, *Phys. Rev. Lett.* **105**, 045503 (2010).
- ⁴⁰J. F. Mercure, R. Karmouch, Y. Anahory, S. Roorda, and F. Schiettekatte, *Phys. Rev. B* **71**, 134205 (2005).
- ⁴¹P. Roura and J. Farjas, *Acta Materialia* **57**, 2098 (2009).
- ⁴²P. Roura and J. Farjas, *Phys. Rev. Lett.* **103**, 119801 (2009).
- ⁴³M. Gibbs, J. Evetts, and J. Leake, *J. Mater. Sci.* **18**, 278 (1983).
- ⁴⁴K. Trachenko, *Phys. Rev. B* **75**, 212201 (2007).
- ⁴⁵K. Trachenko, V. Brazhkin, O. Tsiok, M. T. Dove, and E. Salje, *Phys. Rev. B* **76**, 012103 (2007).
- ⁴⁶K. Trachenko and V. Brazhkin, *J. Phys.: Condens. Matter* **21**, 425104 (2009).
- ⁴⁷J.-F. Joly, Ph.D. thesis, Université de Montréal, 2013.